Size-Dependent Spectroscopy of InP Quantum Dots

O. I. Micić,* H. M. Cheong, H. Fu,† A. Zunger,*,† J. R. Sprague, A. Mascarenhas, and A. J. Nozik*

National Renewable Energy Laboratory, 1617 Cole Boulevard, Golden, Colorado 80401

Received: February 6, 1997; In Final Form: April 11, 1997[X]

The spectroscopic behavior of colloidal InP quantum dots (QDs) has been investigated as a function of the mean QD diameter (which ranged from 26 to 60 Å). Absorption spectra show up to three peaks or shoulders which reflect excited state transitions in the QDs. Global photoluminescence (PL) spectra (excitation well to the blue of the absorption onset and which consequently excites most of the QDs in the size distribution) show broad PL emission. The emission and absorption features shift to higher energy with decreasing QD size. Resonant PL spectra (size-selective excitation into the tail of the absorption onset) show increasing fluorescence line narrowing with increasing excitation wavelength; PL and photoluminescence excitation spectroscopy were used to derive the PL red shift as a function of QD size. The resonant red shifts for QDs of a single size were extracted from PL data that reflect the emission from an ensemble of QD diameters. An analysis of the single-dot resonant red shift (difference between PL peak and the first absorption peak) as a function of the single QD diameter indicate that the results are consistent with a model in which the emission occurs from an intrinsic, spin-forbidden state, split from its singlet counterpart, due to screened electron-hole exchange.

I. Introduction

The spectroscopic properties of semiconductor quantum dots (QDs) are under extensive study because such data provide critical information on the electronic energy level structure of the QDs. A major current issue is the relative importance of the QD surface compared to the QD core structure in controlling the photoluminescence (PL) properties of QDs. In early investigations,[1−7] the predominant view was that the surface structure, especially surface defects, controlled the PL properties; this view was generally accepted because of (i) the exceedingly high surface to volume ratios that are present in small-sized QDs (30% of the atoms in a 35 Å diameter III−V QD are at the surface); (ii) the rather low quantum yield and its dependence on the passivation agent, and (iii) the evidence[6] that at least in Si particles, the red emission involves surface defects. However, recent work[8−14]

of their diameter from the FLN and PLE data that are generated from a distribution of QD sizes.

II. Experimental Section

A. QD Synthesis. Colloidal InP QDs were produced by the following procedure: first, indium oxalate (1.15 g), tris-(trimethylsilyl)phosphine (0.75 g), and a colloidal stabilizer (10 g of a mixture of trioctylphosphine oxide (TOPO) and trioctylphosphine (TOP) in a TOPO:TOP ratio of 0.1:1, were mixed together at room temperature to form a transparent solution of an InP precursor; then, the precursor solution was heated at 250−300 C for 3 days. This procedure produces a colloidal solution of InP QDs that are capped with TOPO/TOP. The TOPO/TOP cap can be replaced with other stabilizers, such as thiols, furan, fatty acids, sulfonic acids, and amines. The QDs can be isolated as a powder by precipitation with methanol; the resultant QD powders can be readily redissolved in nonpolar solvents (such as toulene or a hexane−butanol mixture) to reform transparent colloidal QD dispersions. Fractionation of the QD particles into different sizes can be obtained by selective precipitation methods.[20] X-ray data show that the QD particles have zincblende crystal structure; TEM and electron diffraction data were also consistent with the zincblende InP structure. However, the TEM results were not sufficient to provide detailed information about the specific shape of the QD particles, nor their shape distribution.

Intense band-edge emission from our InP QDs can be achieved after etching the particles with a dilute butanolic solution of HF or NH_4F;[18] 50 íL of the butanolic solution, which contains 5% HF and 10% H_2

which reflect substantial inhomogeneous line broadening arising from the QD size distribution; as expected the spectra shift to higher energy as the QD size decreases. The color of our InP QD samples changes from deep red (1.7 eV) to green (2.4 eV) as the diameter decreases from 60 to 26 Å. Bulk InP is black with a room-temperature band gap of 1.35 eV and an absorption onset at 918 nm. Higher energy transitions above the first excitonic peak in the absorption spectra can also be easily seen in QD samples with mean diameters equal to or greater than 30 Å. For QDs with diameters equal to or greater than 42 Å, a third transition can even be seen in the absorption spectra. The spread in QD diameters is generally about 10% and is

wish to determine. The single-dot emission intensity is thus

where σ_{PL} is the intrinsic broadening of the emission of a single dot, interacting in the ensemble with all other dots. The excitonic gap of a single dot is

where $E_g(\infty)$ is the bulk band gap (1.45 eV for InP at $T = 10$ K or 1.35 at 300 K). For passivated InP dots,[21] $A = 55.2527$ and $n = 1.3611$. The single-dot red shift is taken in the form

where B and m are to be determined from our fit to experiment (see below). The sum over d in eq 2 is limited to those values satisfying $E_g(d) <$ excit, so in effect excit in this equation depends on d.

We fitted the resonant red shift data of Figure 5 for $\langle d \rangle = 32$ Å, using $\sigma_d = 2.5$ Å (the average of the TEM measured values of ref 18), $\sigma_{PL} = 2$ meV, and taking α (,d) to be a constant, over the narrow range of excitation energies involved in Figure 5. Denoting the energy of the peak of the ensemble emission $\bar{I}_{PL}$(, excit, $\langle d \rangle$) as peak (excit, $\langle d \rangle$), we define the "ensemble red shift" as

Figure 6 compares the measured (Figure 5) $\tilde{\phi}$ *vs* excit (diamondlike symbols) to the simulated value (crosses) and shows good agreement. The best fit occurs at

although the fit is somewhat sensitive to the assumed σ

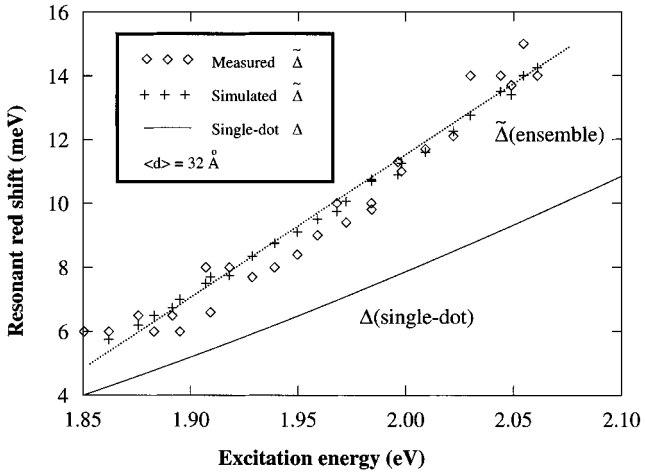

Figure 6. Measured (diamond shaped symbols) ensemble red shift $\tilde{\Delta}$ as a function of excitation energy for $\langle d\rangle = 32$ Å compared with the simulated results (plus signs) using $\sigma_{PL} = 2$ meV, $\sigma_d = 2.5$ Å, $E_g = 1.45 + 55.2527/d^{1.3611}$ and $\alpha(\ ,\ d) =$ const. The single-dot red shift deduced from the simulation (eq 7) is shown as a solid line.

emission narrows, shifts to the red, and has a lower $\tilde{\Delta}(\ _{excit})$ (Figure 7b−e). These trends parallel the observations (Figures 3 and 4). The range of σ_{PL} used in our fit can be narrowed down significantly by requiring that the simulated (half) width of $\bar{I}_{PL}$ shown in Figure 7 agrees with experiment (Figures 3 and 4). This is satisfied at $\sigma_{PL} \cong 2-4$ meV: In Figure 7b, the half-width of the simulated peak is 19 meV, which is close to the experimental value of 21meV measured for an excitation energy of 1.998 eV in Figure 4b. This substantiates our choice $\sigma_{PL} \sim 2$ meV.

While for the $\langle d\rangle = 32$ Å sample we have measured $\bar{I}_{PL}$ by exciting *to the red* of the main absorption peak (i.e., $_{excit} < E_{exciton} \cong 2.17$ eV, see vertical arrow in Figure 5), for the sample with larger average size, $\langle d\rangle \cong 45$ Å, this would necessitate $_{excit} < E_{exciton} \cong 1.86$ eV which is outside our laser range; therefore we had to excite the sample with $\langle d\rangle = 45$ Å by $_{excit} = 1.83-2.0$ eV (Figure 5), i.e., mostly on the *blue side* of the main absorption peak. However, Figure 1 shows that at this excitation energy range, the ~42 Å sample exhibits *two* absorption peaks (denoted "a" and "b"). Thus, this type red shift is no longer "resonant" and our analysis of eq 2 cannot be meaningfully applied to such a high excitation energy experiment. The raw data for the ensemble FLN of $\langle d\rangle = 45$ Å is shown in Figure 5.

Our simulation of the measured FLN spectra suggests a few observations:

(a) Figure 8 shows how the ensemble red shift $\tilde{\Delta}(\ _{excit})$ (calculated with the parameters that fit the measured data of the $\langle d\rangle = 32$ Å sample) approach the single-dot red shift $\Delta(\ _{excit})$ as the size distribution is artificially narrowed in the simulation ($\sigma_d \to 0$). We see that the ensemble and single-dot shifts coincide at a critical excitation energy $_{excit} \sim E_g(\langle d\rangle)$.

(b) Figure 9a compares the measured ensemble red shift $\tilde{\Delta}(\ _{excit})$ (diamondlike symbols) with the simulated result (crosses), in which all parameters (σ_{PL}, σ_d, $\langle d\rangle$, A, n) are held at the values that produced a fit to the data (Figure 6), except that now we set $\Delta(d) \equiv 0$ (compare with Figure 6 in which $\Delta \neq 0$). We see that even though the *intrinsic* red shift is taken as zero, the simulated *ensemble* red shift is nonzero. Clearly, a piece of the ensemble red shift is due to the existence of a size distribution and is unrelated to the spectroscopic characteristics of the individual dots. Figure 9 thus illustrates the importance of removing the spurious red shift $\tilde{\Delta}(\Delta = 0)$ from the measured one, before comparing the results with theory.

Figure 9b further shows the *difference* between the lines of Figure 9a, i.e.,

illustrating that this difference (diamondlike symbols in Figure 9b) is very close to the single-dot red shift deduced from experiment (line in Figure 9b, taken as eq 7). The fact that $\ddot{a}(\ _{excit}) \cong \Delta(\ _{excit})$ suggests a simple way to estimate $\Delta(\ _{excit})$ i.e., use eq 8.

To understand why there is an ensemble red shift even in the absence of a microscopic, single-dot shift we show in Figure 10 the calculated ensemble emission spectra $\bar{I}(\ _{excit})$ for two cases: In Figure 10b we use $\Delta(d) \neq 0$ (after eq 7), illustrating

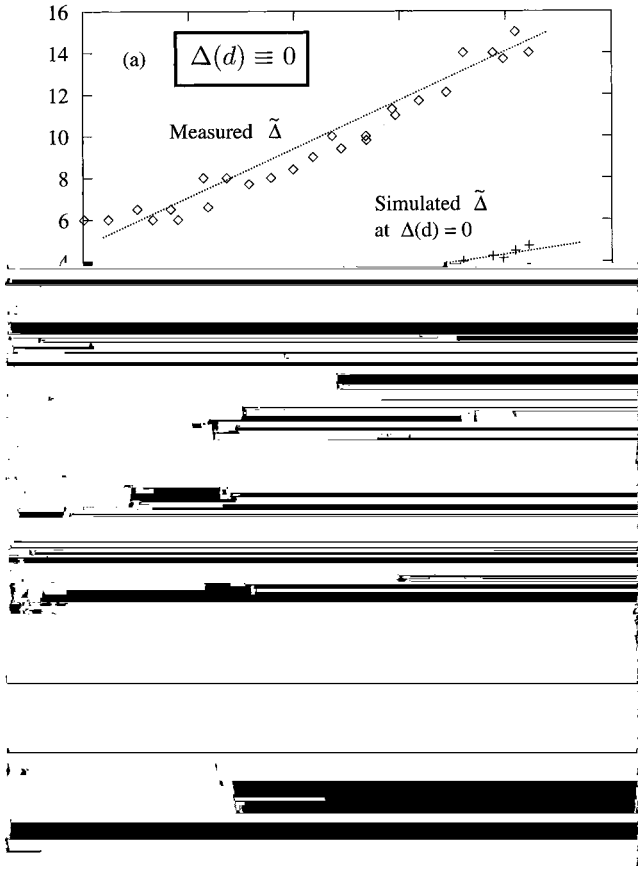

Figure 9. (a) Measured $\tilde{\phi}_{measured}(\ _{excit})$ ensemble red shift for $\langle d \rangle = 32$ Å (diamond-shaped symbols), compared with the simulated $\tilde{\phi}_{simulated}$-$(\ _{excit};\ \phi \equiv 0)$ ensemble red shift (plus signs) assuming $\phi(d) \equiv 0$. (b) The difference $\ddot{a}(\ _{excit}) = \tilde{\phi}_{measured} - \tilde{\phi}_{simulated}\ (\phi = 0)$ (diamond-shaped symbols) compared with the single-dot red shift $\phi(d)$ of eq 7 (solid line).

how the individual, single-dot emission peaks a, b, and c produce the ensemble emission that is red-shifted with respect to the excitation energy (vertical line). If we now move the excitation energy to coincide with the emission peak of *one particular dot size* (peak a in Figure 10a, where $\phi \equiv 0$), the *other* dots emit "out of resonance", so still $\phi \neq 0$.

Figure 11 shows the simulated red shift for a few assumed average sizes $\langle d \rangle = 20$, 32 Å. We use $\acute{o}_d = 2.0$ and 2.5 Å, respectively. We see that $\tilde{\phi}(\ _{excit}, \langle d \rangle)$ *vs* $_{excit}$ has an *increasing slope* as $\langle d \rangle$ increases, even though all of these curves have an identical underlying single-dot red shift $\phi(d)$. Thus, even though the *single-dot* red shift *increases* as the dot size is reduced (eq 7), the *ensemble* red shift *decreases* as the dot size is reduced. This illustrates further that the measured ensemble red shift should not[8,9,11−13] be compared directly with a calculated $\phi(d)$.

Finally, Figure 12 shows the single-dot red shift deduced from our experiments. This quantity should be directly compared to the prediction of theoretical models.

D. PL Lifetime. The PL lifetimes were measured in a sample of HF-treated InP QDs immobilized in a PVB film at 298 K and 13 K; the mean QD diameter was 30 Å. The PL decay as a function of time for this sample is shown in Figure 13; excitation was at 585 nm and the emission was monitored at 620 nm. The decay is multiexponential; the data were fit to three exponentials, and the results are presented in Table 1. At 298 K most of the decay (91%) can be described by two time constants of 28 and 73 ns; at 13 K most of the decay (98%) can be described by time constants of 173 and 590 ns.

IV. Discussion

Our results show that for InP QDs formed via collodial chemical processes, very large effects due to a residual QD size distribution remain manifested in the photoluminescence spectroscopy of QD ensembles even after the colloidal samples have been subjected to size-selective precipitation techniques and size-selective photoexcitation. This behavior is similar to that reported for colloidal CdSe QD ensembles.[8−14]

When the colloidal samples are photoexcited well to the blue of the absorption onset, so that most of the QDs in the size

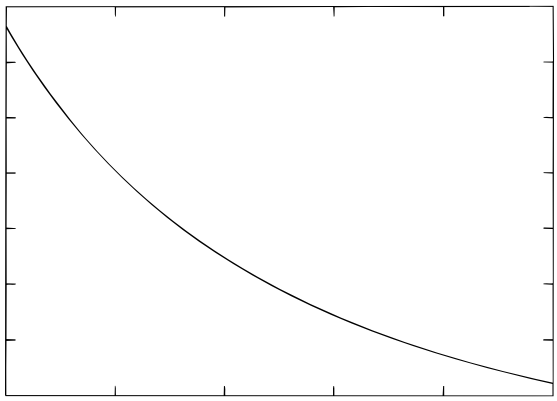

distribution are excited, the resulting global PL shows a very broad peak (line width of 175−225 meV) that is red-shifted by 100−300 meV from the first absorption peak (Figures 1, 2, and 3f). The broad PL line width is caused by inhomogeneous line broadening arising from the ∼10% size distribution sampled in the global PL experiment, as seen from the simulation (trace a in Figure 7). The large global red shift is caused by the volume dominance of the larger particles in the size distribution; the larger QDs will absorb most of the incident photons and will also show large red shifts since the PL excitation energy is well above their lowest transition energy.

As seen in Figures 3 and 4, the PL obtained by exciting into the red tail of the QD absorption spectrum, and thereby selectively exciting only the largest particles in the distribution, shows much smaller line widths (15−30 meV) and smaller red shifts compared to the global PL (compare Figures 2 and 5). However, as our analysis shows in Figures 6−12, even the size-selected PL/FLN spectra contain effects due to a residual size distribution. We have extracted the resonant red shifts for QDs of a single size from the experimental PL/FLN spectra using the approach described in Section III. The results of this analysis (see solid line in Figure 6 and Figure 12) show that the effective single-dot resonant red shift at 10 K exhibited by InP quantum dots that have been etched in HF to passivate surface states ranges from 4 meV for an excitation energy of 1.85 eV (corresponding to a QD size of 53 Å) to 9.7 meV for an excitation energy of 2.06 eV (corresponding to a QD size of 34 Å).

The origin of the resonant red shift in InP has been recently analyzed theoretically.[15,21] The methodology used was to treat a passivated quantum dot as a "giant molecule" in its own right, rather than an object drawn from an infinite crystal surrounded by an infinite potential barrier.[8,9,11−13] To this end, infinite-barrier **k•p** approaches[8,9,11−13] were avoided in favor of a pseudopotential super-cell approach,[15,21] in which a dot of any selected shape and size is modeled explicitly, and passivating atoms decorate all surface sites. To examine possible surface effects, cation-passivants and anion-passivants were selectively removed, and the electron structure was recalculated. Four possible models have been examined as to their ability to explain the resonant red shift: (1) emission from an intrinsic, spin-forbidden state, split from its singlet counterpart due to screened electron-hole exchange; (2) emission from an intrinsic, orbitally-forbidden conduction band state e.g., X_{1c} (rather than ¡ Ic); (3) emission to an intrinsic, orbitally-forbidden valence band state (e.g., p-like); and (4) emission from extrinsic surface defects (e.g., surface vacancies). The experimental results reported here are quantitatively consistent with model 1 when the exchange interactions are screened by a distance-dependent[22] dielectric function[15] (see refs 23−25 for discussion of exchange screening). In model 1, an enhanced (relative to bulk) electron-hole exchange interaction splits the exciton state into a lower energy spin-forbidden state (triplet) and a higher energy spin-allowed singlet. Absorption occurs into the upper state, followed by relaxation to and emission from the lower state; the difference between these two states is the resonant red shift.[8−15] The value of the single-dot resonant red shift (as a function of QD size) derived from the experimental data is in excellent agreement with the theoretical predictions.[15]

Model 2 was rejected[15] because it was shown that the conduction band minimum in InP dots is not derived from an indirect X_{1c}-like state as in small GaAs particles,[15] and model 3 was rejected[15] because the symmetry of the envelope function of the valence band maximum was found to be 1s-like and not 1p-like as expected from simple **k•p** models. Model 4 shows that *fully* passivated QDs have no surface states, despite the large surface-to-volume ratio. However, in the event that some of the surface atoms were not capped by a passivant (due to, e.g., steric-hindrance by large passivating molecules), model 4 shows that surface *defect states* (due to surface uncapped In or surface uncapped *P*) could appear inside the QD band gap. These surface defects lead to large red shifts extending from one hundred to a few hundred meV depending on the surface conditions; such large red shifts are observed in unetched InP QDs but are removed upon HF etching.[18] The magnitude of the observed resonant red shifts reported here after etching is not consistent with the surface defects present in the initial QD synthesis; these are removed or passivated and do not affect the PL. While surface defect states do not explain the e 10 meV *resonant* red shift, direct theoretical modeling of such states[15] show that they affect (i) the quantum-efficiency (through nonradiative recombination), and (ii) lead to a significant hybridization with the ordinary, corelike band edge states, thus affecting the radiative emission rate from theses states. Furthermore, since these hybridized states reflect the properties of the uncapped site (i.e., P or In "dangling bond") rather than those of the passivating molecules around this site, it was

predicted[15] that surface defect states are mostly independent of the passivant and have size-dependent lifetimes. The degree of mixing of surface defect wavefunctions with the ordinary

(3) Hasselbarth, A.; Eychmuller, A.; Weller, H. *Chem. Phys. Lett.* **1993**, *203*, 271.
(4) Bawendi, M. G.; Carroll, P. J.; Wilson, W. L.; Brus, L. E. *J. Chem. Phys.* **1992**, *96*, 946.
(5) Nirmal, M.; Murray, C. B.; Bawendi, M. G. *Phys. Rev. B* **1994**, *50*, 2293.
(6) Petrova-Koch, V.; Muschik, T.; Kux, A.; Meyer, B. K.; Koch, F.; Lehmann, V. *Appl. Phys. Lett.* **1992**, *61*, 943.
(7) Hoheisel, W.; Colvin, Y. L.; Johnson, C. S.; Alivisatos, A. P. *J. Chem. Phys.* **1994**, *101*, 845.
(8) Nirmal, M.; Norris, D. J.; Kuno, M.; Bawendi, M. G.; Efros, A. L.; Rosen, M. *Phys. Rev. Lett.* **1995**, *75*, 3728.
(9) Efros, A. L.; Rosen, M.; Kuno, M.; Nirmal, M.; Norris, D. J.; Bawendi, M. *Phys. Rev. B* **1996**, *54*, 4843.
(10) Norris, D. J.; Bawendi, M. G. *Phys. Rev. B* **1996**, *53*, 16338.